Engineering Analysis with Boundary Elements **10** (1992) 59–68

Stress intensity factors for cracks around or penetrating an elliptic inclusion using the boundary element method

Y.L. Gao, C.L. Tan & A.P.S. Selvadurai

Faculty of Engineering, Carleton University, Ottawa, Canada K1S 5B6

In this paper, methods for directly evaluating stress intensity factors using quadratic quarter-point crack-tip elements in two-dimensional Boundary Element analysis are reviewed. They include those for treating cracks which lie along the interface between dissimilar materials. Using these methods, stress intensity factors are obtained for three general crack problems, all involving an elastic elliptic inclusion in an infinite matrix. Numerical results are presented for a range of geometric parameters; the effects of the mismatch of the shear modulus of the inclusion and that of the matrix are also considered.

INTRODUCTION

In recent years, there has been increasing attention paid to the study of cracks approaching, terminating, crossing, or lying along bimaterial interfaces, see, e.g. Refs 1–14. Solutions to these problems have important applications in geomechanics, biomechanics, and, generally, the study of failure of multiphase (metallurgic or composite) materials. The range of problems that may be encountered, even in two dimensional elasticity alone, which is the scope of the present paper, is very broad indeed. Among them is a class which features an inclusion or inclusions embedded in an elastic matrix with cracks present. Studies in this area include those by England,[15] Perlman & Sih,[16] Toya,[17,18] Sendeckyj,[19] Erdogan *et al.*,[20] Selvadurai & Singh,[21] Erdogan & Gupta,[4] Viola & Piva,[5] Hasebe *et al.*,[12] Steif,[11] and Liu & Erdogan.[10] Most of these analytical studies are concerned with either a crack lodged in an inclusion or that occurring at the interface between the inclusion and the matrix. The method of analysis employed can generally be categorised into either mapping techniques using complex function theory, or the integral equation approach whereby a set of singular integral equations is derived and solved numerically in order to evaluate the stress intensity factors for the crack.

Engineering Analysis with Boundary Elements 0955-7997/92/$05.00

Numerical methods of stress analysis provide alternative means of examining this class of crack-inclusion problems. Among the computational methods, the finite element method and the boundary element method (BEM), also often known as the boundary integral equation (BIE) method, have been well established for the stress analysis of cracked homogeneous bodies. The use of the former method has also been fairly extensive for treating crack problems in composite materials, see, e.g. Refs 22–28. On the other hand, the application of the BEM in this area has, to date, been extremely limited indeed, and it has been mainly confined to bimaterial interface crack problems.[29–35] For cracks with crack-tips located within piece-wise homogeneous and isotropic regions, the determination of the stress intensity factors, K_I and K_{II}, using BEM is a relatively straightforward procedure. To this end, the techniques which have been successfully established for treating cracked homogeneous bodies could equally be applied here since the stress singularity at the crack tip remains the conventional $r^{-1/2}$ form. For cracks which lie along the interface between two dissimilar materials, the stress singularity, although also of the $r^{-1/2}$ form, is highly oscillatory in manner as the crack-tip is approached. This presents some difficulties in conventional BEM modelling of the problem. Lee & Choi,[34] for example, resorted to using extremely refined meshes to obtain the stress intensity factors by the conventional BEM, while Yuuki *et al.*[30–32] and Hasegawa[33] employed

special fundamental solutions in their BIE formulations for treating the problem. Tan & Gao[35] recently examined the use of the conventional BEM in conjunction with quarter-point crack-tip elements, similar to those used for analysing cracked homogeneous bodies, for such problems. They derived expressions for evaluating the stress intensity factor directly from the displacement data for the crack-tip elements or from the computed traction at the crack tip, and found that good accuracy of the stress intensity factor solution could be obtained even with relatively coarse mesh discretisations.

In this paper, the conventional multi-region boundary element method with quarter-point crack-tip elements is used to obtain stress intensity factors for a finite size crack in an elastic matrix which also spans partially around an elastic elliptical inclusion at the interface. The case of the crack having either partially or wholly penetrated the inclusion is also analysed in this study. A relatively wide range of geometric parameters is considered and the effects of the mismatch of material properties between the inclusion and the matrix are investigated. In the following section, the techniques for directly evaluating stress intensity factors using BEM are briefly reviewed. Numerical results for the problems treated are then presented and discussed.

DIRECT EVALUATION OF STRESS INTENSITY FACTORS USING BEM

The analytical and numerical formulation of the boundary element method is well documented in the literature, see, e.g. Refs 36 and 39. For a homogeneous and isotropic elastic domain, the direct boundary integral equation (BIE) relating the displacements u_i and the tractions t_i at the boundary S, in Cartesian coordinates x_i, may be written, using indicial notation, as:

$$C_{ji}(P)u_i(P) + \int u_i(Q)T_{ji}(P,Q)\,\mathrm{d}S(Q) = \int t_i(Q)U_{ji}(P,Q)\,\mathrm{d}S(Q) \qquad i,j = 1,2 \tag{1}$$

In eqn (1), $U_{ij}(P,Q)$ and $T_{ij}(P,Q)$ are the fundamental solutions for the displacements and tractions, respectively, for the well-known Kelvin problem. Also, the value of $C_{ij}(P)$ depends on the local geometry of S at P and is equal to $1/2\ \delta_{ij}$, where δ_{ij} is the Kronecker delta, if P lies on the smooth part of S.

To solve the BIE numerically, the boundary S is first discretised into a series of, say, M line elements. Over each of these elements, the geometry, displacements and tractions may be assumed to vary according to a simple polynomial. In this study, the quadratic isoparametric variation is assumed, thus, over each of the three-noded elements,

$$x_i(\xi) = \sum_{c=1}^{3} N^C(\xi)x_i^c$$

$$u_i(\xi) = \sum_{c=1}^{3} N^C(\xi)u_i^c$$

$$t_i(\xi) = \sum_{c=1}^{3} N^C(\xi)t_i^c \tag{2}$$

In eqn (2), the superscript c denotes the local node number, ξ is the intrinsic coordinate ($-1 \le \xi \le +1$), and $N^C(\xi)$ are the quadratic shape functions given by

$$N^1(\xi) = \tfrac{1}{2}\xi(\xi - 1)$$

$$N^2(\xi) = 1 - \xi^2$$

$$N^3(\xi) = \tfrac{1}{2}\xi(\xi + 1) \tag{3}$$

Substitution of eqn (2) into eqn (1) results in the discretised form of the BIE, namely,

$$C_{ji}(P^a)u_j(P^a) + \sum_{b=1}^{N}\sum_{c=1}^{3} u_j(P^{d(b,c)}) \int_{S_b} T^{ji}(P^{d(b,c)}, Q) \times N^c(\xi)J(\xi)\,\mathrm{d}\xi = \sum_{b=1}^{M}\sum_{c=1}^{3} t_j(P^{d(b,c)}) \int_{S_b} U_{ji}(P^{d(bc,0)}, Q)N_c(\xi)1J(\xi)\,\mathrm{d}\xi \qquad p^a = 1, N \tag{4}$$

where N is the total number of distinct nodes on S, $J(\xi)$ is the Jacobian of transformation from the global to local coordinates, and $P^{d(b,c)}$ denotes the cth node of the bth element.

For problems in which there are piece-wise homogeneous regions of different material properties, eqn (1) and (4) may be written for each sub-region in turn and the compatibility conditions applied at the sub-region interface boundaries. Equation (4), or its modified form for multi-regions, represent a set of N linear algebraic equations for the unknown nodal values of displacements or tractions at the boundary S. They may be solved using, for example, Gaussian elimination.

When using the finite element method with quadratic isoparametric elements, it is well known that a simple way to represent the $r^{1/2}$ and $r^{-1/2}$ displacement and traction variations, respectively, in the vicinity of the crack-tip is to place the mid-side nodes to the quarter-points, see Fig. 1.

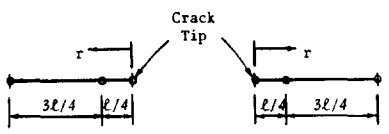

Fig. 1. Quadratic quarter-point crack-tip elements.

In BEM however, because the displacements and tractions are independently represented, their variations in such a quarter-point element, when using the shape functions given in eqn (3), are of the same form, namely,

$$\left.\begin{matrix} u_i \\ t_i \end{matrix}\right\} = A_i^1 + A_i^2\sqrt{\frac{r}{l}} + A_i^3\left(\frac{r}{l}\right) \tag{5}$$

where the A_i^n are constants for the element. To achieve the proper $r^{-1/2}$ singularity for the traction variation, the right-hand-side of eqn (5) may be multiplied by (l/r), l being the length of the crack-tip element. Thus,

$$t_i = \left[A_i^1 + A_i^2\sqrt{\frac{r}{l}} + A_i^3\left(\frac{r}{l}\right)\right]\left(\sqrt{\frac{l}{r}}\right)$$

$$= \frac{B_i^1}{\sqrt{\frac{r}{l}}} + B_i^2 + B_i^3\sqrt{\frac{r}{l}} \tag{6}$$

In terms of the shape functions, (6) may be written as

$$t_i = \bar{t}_i^1 N^1(\xi)\sqrt{\frac{l}{r}} + \bar{t}_i^2 N^2(\xi)\sqrt{\frac{l}{r}} + \bar{t}_i^3 N^3(\xi)\sqrt{\frac{l}{r}}$$

$$= \bar{t}_i^1 \bar{N}^1(\xi) + \bar{t}_i^2 \bar{N}^2(\xi) + \bar{t}_i^3 \bar{N}^3(\xi) \tag{7}$$

where $\bar{t}_i^n$ denotes the nodal values of t_i divided by the nodal values of $\bar{N}^n(\xi)$. It can be easily verified that for this quarter-point element,

$$\bar{t}_i^3 = t_i^3$$

$$\bar{t}_i^2 = \tfrac{1}{2}t_i^2$$

$$\bar{t}_i^1 = \lim_{r\to 0} t_i^1\sqrt{\frac{r}{l}} \tag{8}$$

To treat a general crack problem involving mixed mode deformation in a homogeneous body using the conventional BEM, the physical domain may be represented by two or more sub-regions such that the crack planes coincide wth the sub-region interface boundaries.[37] Using the quarter-point crack-tip elements described above, the stress intensity factors can be obtained directly using either the computed values of the nodal displacements for the crack-tip elements on the crack faces, or from the computed value of t_i^1 at the crack-tip for the traction singular quarter-point element ahead of the tip. Expressions for such direct evaluation of the stress intensity factor may be obtained[37,38] by equating the classical near-tip field solution to eqn (5) or eqn (6) respectively. With reference to Fig. 2, these expressions are given below:

Displacement formula

$$K_I = \frac{\mu}{(\kappa+1)}\sqrt{\frac{2\pi}{l}}[4(u_2^B - u_2^D) + (u_2^E - u_2^C)]$$

$$K_{II} = \frac{\mu}{(\kappa+1)}\sqrt{\frac{2\pi}{l}}[4(u_1^B - u_1^D) + (u_1^E - u_1^C)] \tag{9}$$

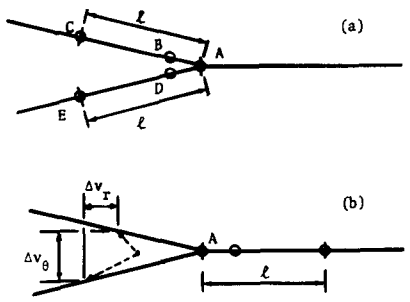

Fig. 2. (a) Quarter-point elements on crack faces. (b) Quarter-point elements ahead of crack-tip.

where

$$\kappa = \begin{cases} 3 - 4\nu & \textit{for plane strain} \\ \dfrac{3-\nu}{1+\nu} & \textit{for plane stress} \end{cases} \tag{10}$$

In eqns (9) and (10), μ and ν are the shear modulus and Poisson's ratio, respectively.

Traction formula

$$K_I = \bar{t}_2^A\sqrt{2\pi l}$$

$$K_{II} = \bar{t}_1^A\sqrt{2\pi l} \tag{11}$$

where the superscripts denote the nodal points shown in Fig. 2.

It has been demonstrated, see, e.g. Ref. 38, that even when using relatively coarse mesh discretisations, very accurate stress intensity factor solutions can be obtained with these formulas.

To treat bimaterial interface crack problems using BEM, the multi-region approach for treating general crack problems in homogeneous bodies may be followed, with each sub-region in the BEM model representing each piece-wise homogeneous part of the physical problem. However, eqns (9) and (11) cannot be applied to determine the stress intensity factors for the interface crack. This is because the singular stress fields are oscillatory in form as the interface crack-tip is approached.[40] Associated with these stresses is the physically inadmissible feature of interpenetration of the crack faces. This issue was resolved by Comninou[41] who showed this to be a consequence of not taking into consideration the contact conditions between the crack faces, albeit over only a very small zone, at the interface crack-tip. As pointed out again recently by Rice,[42] although this implies that the oscillatory field solutions are not valid on the scale of the contact zone, they do still provide a proper characterising parameter for the near-tip state when, as in most typical circumstances, that zone is extremely small compared to the crack size.

When treating bimaterial interface cracks, it is convenient then to introduce K, the complex stress

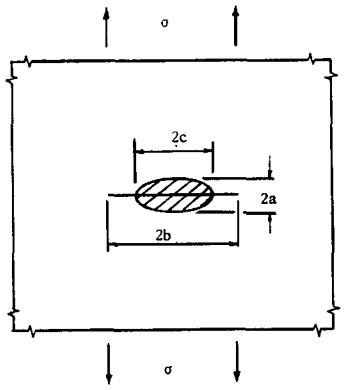

Fig. 3. Problem (I).

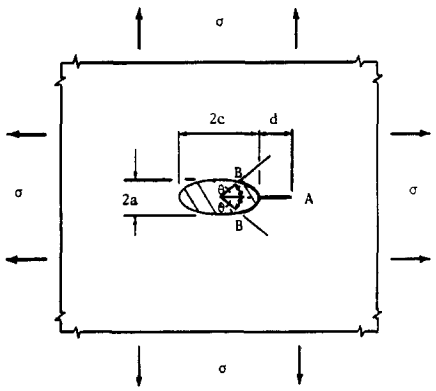

Fig. 5. Problem (III).

intensity factor defined by:

$$K = K_I + iK_{II} \tag{12}$$

The stresses at distance r ahead of the crack-tip are related to this complex stress intensity factor by

$$\frac{1}{\cos h\pi\epsilon}(\sigma_{\theta\theta} + i\tau_{r\theta})|_{\theta=0} = \frac{Kr^{-i\epsilon}}{\sqrt{2\pi r}} \tag{13}$$

In eqn (13), the stresses $\sigma_{\theta\theta}$ and $\tau_{r\theta}$ are with respect to a local polar co-ordinate system with the origin at the crack-tip; the bonded interface corresponds to $\theta = 0$ and the free crack faces of material 1 and material 2 are defined by $\theta = -\pi$ and $\theta = \pi$ respectively. Also

$$\epsilon = \frac{1}{2\pi}\ln\frac{\mu_1 + \kappa_1\mu_2}{\mu_2 + \kappa_2\mu_1} \tag{14}$$

is the bimaterial constant where the subscripts denote the material type number. It should be noted that because the tensile and shear effects are coupled near the interface crack-tip, K_I and K_{II} here cannot be defined in the classical separate form as for homogeneous materials (see, e.g. Ref. 43). The complex stress intensity factor as defined above may also be written as

$$K = K_o e^{i\Psi} \tag{15}$$

where K_o and Ψ are the modulus and argument, respectively, of the complex stress intensity factor. Thus

$$K_o = |K| = \sqrt{K_I^2 + K_{II}^2} \tag{16}$$

$$\Psi = \tan^{-1}(K_{II}/K_I) \tag{17}$$

It can be shown (see, e.g. Ref. 44) that the maximum amplitude of the singular stresses in the vicinity of the crack-tip is determined by K_o, and unlike K_I and K_{II}, K_o is not oscillatory in form. It can further be shown that the strain energy release rate is directly proportional to K_o^2. The fact that K_o is not oscillatorily singular means that its determination is less likely to suffer numerical resolution difficulties as would be the case if K_I and K_{II} are to be determined directly here. Knowledge of K_o and Ψ for a given cracked configuration and loading condition will however enable the near tip stress state to be related to some crack extension criterion.

Using the quarter-point crack-tip elements described earlier and employing similar procedures for deriving eqns (9) and (11), expressions equivalent to these equations for directly obtaining K_o for the bimaterial interface crack may also be obtained.[35] They are, with reference to Fig. 2, given below:

Displacement formula

$$K_o = \sqrt{\frac{2\pi}{l}}[W^2 + V^2]^{1/2} \tag{18}$$

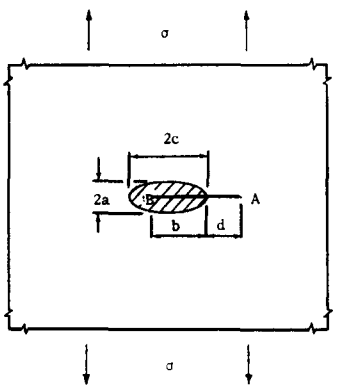

Fig. 4. Problem (II).

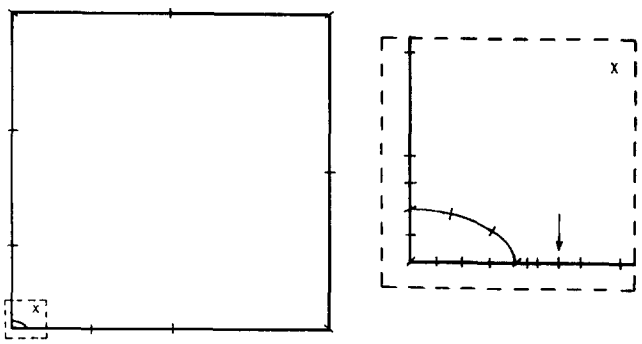

Fig. 6. Typical BEM mesh for Problem (I).

Table 1. Normalised stress intensity factors, $K_1/\bar{K}$, for Problem (I), $\bar{K} = \sigma\sqrt{\pi b}$

c/a	b/c	μ_2/μ_1			
		5	10	20	100
	1·05	1·571	1·781	1·933	2·093
	1·10	1·534	1·741	1·889	2·045
	1·20	1·237	1·315	1·367	1·419
1/3	1·40	1.112	1·149	1·173	1·197
	1.50	1·089	1.117	1·135	1·153
	1.60	1·068	1·089	1·102	1·116
	1·80	1·036	1·048	1·056	1·064
	1·05	1·402	1·547	1·651	1·760
	1·10	1·285	1·380	1·446	1·514
	1.20	1.159	1·211	1·247	1·283
1/2	1·40	1·060	1·082	1·097	1·112
	1·50	1·047	1·062	1·073	1·084
	1·60	1·033	1·044	1·052	1·060
	1·80	1·013	1·019	1·023	1·028
	1·05	1·261	1·363	1·442	1·530
	1·10	1·148	1·208	1·255	1·308
1	1·20	1·058	1·088	1·112	1·139
	1·40	1·005	1·015	1·024	1·035
	1·50	1·002	1·012	1·018	1·026
	1·60	1·000	1·005	1·009	1·015
	1·05	1·111	1.180	1·259	1·409
	1·10	1·026	1·058	1·099	1·179
2	1·20	0·995	1·008	1·027	1·066
	1·40	0·984	0·987	0·994	1·008
	1·60	0·995	0·996	0·999	1·006
	1·05	1·032	1·065	1·120	1·289
	1·10	0·989	1·002	1·028	1·113
3	1·20	0·985	0·988	0·999	1·038
	1·40	0·993	0·992	0·995	1·009

where

$$W = D_1[-u_1^E + 4u_1^D - 3u_1^A] - D_2[-u_1^C + 4u_1^B - 3u_1^A] \tag{19}$$

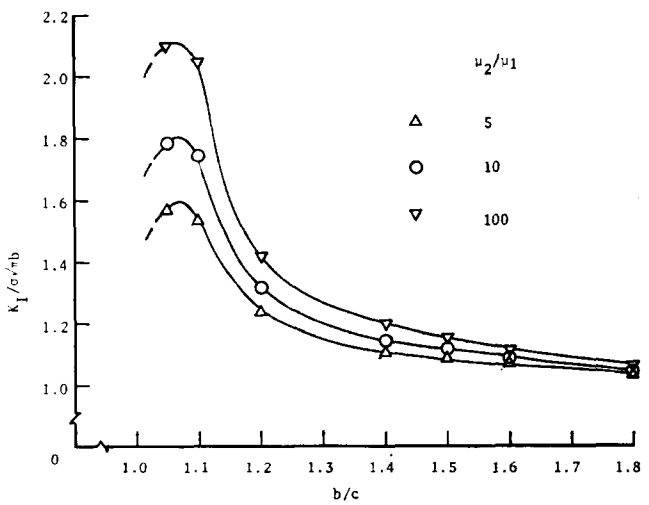

Fig. 7. Variation of $K_I/\sigma\sqrt{\pi b}$ with b/c for Problem (I); $c/a = 1/3$.

$$V = D_1[-u_2^E + 4u_2^D - 3u_2^A] - D_2[-u_2^C + 4u_2^B - 3u_2^A] \tag{20}$$

$$D_1 = \frac{(1+\gamma)\lambda_0}{\cos h(\pi\epsilon)} \cdot \frac{\mu_1}{\kappa_1 e^{\pi\epsilon} + \gamma e^{-\pi\epsilon}} \tag{21}$$

$$D_2 = \frac{(1+\gamma)\lambda_0}{\cos h(\pi\epsilon)} \cdot \frac{\mu_2}{\kappa_2\gamma e^{-\pi\epsilon} + e^{\pi\epsilon}} \tag{22}$$

$$\lambda_0 = (\tfrac{1}{4} + \epsilon^2)^{1/2} \tag{23}$$

In the above equations, l is the length of the crack-tip elements as shown in Fig. 2, and the superscripts denote the nodal points shown in the same figure.

Traction formula

$$K_0 = \frac{\sqrt{2\pi l}}{\cos h(\pi\epsilon)}[(\bar{t}_1^A)^2 + \bar{t}_2^A)^2]^{1/2} \tag{24}$$

where $\bar{t}_1^A$ denotes the BEM computed traction at the crack-tip node.

To obtain the phase angle Ψ from numerical data, use may be made of its relationship with the crack-face opening displacements. It can be shown, (see, e.g. Ref. 23), that

$$\Psi = \tan^{-1}(\Delta v_r/\Delta v_\theta) + \epsilon \ln r - \tan^{-1}(2\epsilon) \tag{25}$$

where Δv_r and Δv_θ are the crack opening displacements between the crack faces in the r- and θ-directions at distance r from the interface crack-tip. Note however that Ψ is scale dependent.[42] Thus for its results to be generally applicable, it should be presented in a scale-invariant form, such as

$$Kh^{-i\epsilon} = K_0 e^{i\Psi^*} \tag{26}$$

where

$$\Psi^* = \Psi - \epsilon \ln h$$

$$= \tan^{-1}(\Delta v_r/\Delta v_\theta) + \epsilon \ln (r/h) - \tan^{-1}(2\epsilon) \tag{27}$$

The parameter h in the above equations may be any characteristic dimension of the problem. It is evident here that Ψ^* cannot be evaluated numerically at the crack-tip itself, that is at $r = 0$. Numerical experiments

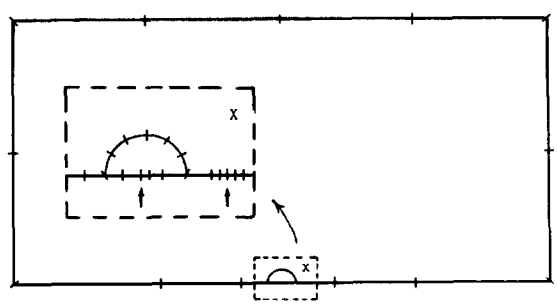

Fig. 8. Typical BEM mesh for Problem (II).

Table 2a. Normalised stress intensity factors, $K_A = (K_I)_A/\bar{K}$, for point A in Problem (II), $\bar{K} = \sigma\sqrt{\pi(b+d)}$

c/a	$b/2c$	μ_2/μ_1			
		5	10	20	100
	0·02	0·565	0·463	0·400	0·341
	0·35	0·590	0·481	0·407	0·324
1/3	0·50	0·634	0·526	0·445	0·333
	0·65	0·665	0·559	0·480	0·357
	0·80	0·718	0·619	0·544	0·435
	0·20	0·639	0·556	0·504	0·454
	0·35	0·662	0·569	0·504	0·426
1/2	0·50	0·711	0·617	0·543	0·429
	0·65	0·738	0·656	0·587	0·450
	0·80	0·791	0·721	0·666	0·547
	0·20	0·771	0·717	0·681	0·644
	0·35	0·783	0·717	0·665	0·598
1	0·50	0·826	0·759	0·695	0·587
	0·65	0·841	0·786	0·728	0·589
	0·80	0·882	0·844	0·806	0·678
	0·20	0·873	0·837	0·807	0·766
	0·35	0·882	0·841	0·800	0·722
2	0·50	0·915	0·874	0·831	0·722
	0·65	0·911	0·879	0·842	0·724
	0·80	0·935	0·911	0·884	0·785
	0·20	0·909	0·882	0·857	0·811
	0·35	0·919	0·891	0·861	0·782
3	0·50	0·947	0·921	0·891	0·798
	0·65	0·937	0·915	0·891	0·805
	0·80	0·954	0·935	0·915	0·843

Table 2b. Normalised stress intensity factors, $K_B = (K_I)_B/\bar{K}$, for point B in Problem (II), $\bar{K} = \sigma\sqrt{\pi(b+d)}$

c/a	$b/2c$	μ_2/μ_1			
		5	10	20	100
	0·20	1.697	1.945	2·144	2·418
	0·35	1·984	2·424	2·859	3.673
1/3	0·50	2.223	2·844	3·563	5·425
	0·65	2·364	3·112	4.052	7·443
	0·80	2·675	3·582	4.700	10·026
	0·20	1·706	1.962	2·163	2·406
	0·35	1·990	2·457	2·910	3·613
1/2	0·50	2.219	2·905	3·713	5·443
	0·65	2·366	3·206	4·348	7·975
	0·80	2·645	3·607	4·948	11·283
	0·20	1.684	1·961	2·179	2·432
	0·35	1·945	2·431	2·888	3·534
1	0·50	2·155	2·867	3·677	5·186
	0·65	2·279	3·169	4·380	7·698
	0·80	2·483	3·486	5·008	11·784
	0·20	1·846	2·323	2·799	3·528
	0·35	2·008	2·646	3.399	4·958
2	0·50	2.138	2.890	3·867	6·533
	0·65	2·212	3·046	4·189	8·190
	0·80	2·413	3·398	4·789	10·862
	0·20	1·944	2.551	3·263	4·690
	0·35	2.049	2·757	3·686	6·370
3	0·50	2·150	2·934	3·990	7·720
	0·65	2·175	2·991	4·097	8·494
	0·80	2·364	3.330	4·664	10·179

using BEM on several different well-known test problems have shown however that to obtain accurate estimates of Ψ^*, a very good position to apply eqn (27) is at the mid-point of the crack-tip elements. This is true for a wide range of relative crack-tip element sizes, from $l/a = 0{\cdot}02$ to $0{\cdot}15$, where a is the modelled crack length.

NUMERICAL RESULTS

The BEM results presented here are for an infinite elastic matrix of material (1) which has an embedded elliptic inclusion of material (2), with semi-axes a and c. Three different situations of crack occurrence were considered in this study; they are shown in Figs 3–5 as Problems (**I**), (**II**) and (**III**), respectively. In each of these main set of problems, five different geometries of the elliptic inclusion were treated. They are $c/a = 1/3$, 1/2, 1, 2 and 3, with a range of crack sizes analysed for each. For a given crack configuration, the effects of the mismatch of material properties between the inclusion and the matrix were also investigated. To this end, four different values of the shear modulus ratios μ_2/μ_1 were treated, namely, 5, 10, 20 and 100; the Poisson's ratio of both materials were taken to be the same, however, as 0·3. Plane strain conditions were assumed throughout.

In the numerical models employed, the infinite matrix was represented as a square domain with side lengths twenty times the length of the major axis of the elliptic inclusion. Quarter-point crack-tip elements were used in all the analyses. For evaluating the stress intensity factors, both the displacement formulas and the traction formulas presented above were used. It was found that the deviations of the stress intensity factor results obtained from these formulas were generally less than two percent. The traction formulas have been shown to yield solutions which are less sensitive to crack-tip element size however,[37,38] thus only this set of results are presented below. Also, for Problems (**I**) and (**II**), when materials 1 and 2 are taken to be identical, the problems reduce to that of a crack in an infinite homogeneous body. The accuracy of the numerical stress intensity factor solutions obtained with every mesh employed in Problems (**I**) and (**II**) was checked for this case and found to be indeed excellent, with error of less than one percent in general. Although this level of accuracy is unlikely to be maintained for the non-homogeneous cracked bodies, particularly those involving interfacial cracks in Problem (**III**), as experience in Ref. 35 has shown, the errors in the numerical solutions are expected to be within 5 percent of the true values.

Problem (I)

In this problem, see Fig. 3, a crack of length 2b has completely penetrated the elliptic inclusion along one of its axes and the two crack-tips are located in the matrix symmetric about the inclusion. The matrix is subjected

Table 3a. Normalised stress intensity factors, $K_A^* = (K_I)_A/\bar{K}$, for point A in Problem (III), $\bar{K} = \sigma\sqrt{\pi d}$

c/a	0	μ_2/μ_1			
		5	10	20	100
	30°	0·599	0·562	0·541	0·521
	60°	0·553	0·522	0·509	0·503
1/3	90°	0·665	0·634	0·610	0·583
	120°	0·798	0·794	0·793	0·790
	30°	0·633	0·607	0·593	0·581
	60°	0·669	0·648	0·639	0·634
1/2	90°	0·881	0·856	0·841	0·825
	120°	1·034	1·028	1·024	1·020
	30°	0·711	0·696	0·689	0·683
	60°	0·844	0·829	0·821	0·815
1	90°	0·996	0·982	0·974	0·967
	120°	1·128	1·119	1·113	1·109
	30°	0·803	0·794	0·789	0·785
	60°	0·925	0·917	0·912	0·908
2	90°	1·004	0·996	0·992	0·988
	120°	1·081	1·074	1·070	1·067
	30°	0·854	0·848	0·844	0·841
	60°	0·949	0·942	0·939	0·936
3	90°	1·002	0·996	0·993	0·990
	120°	1·054	1·049	1·046	1·044

to uniform tension σ at the remote ends in the direction perpendicular to the plane of the crack. Figure 6 shows a typical BEM mesh used for the analysis of this problem. Only one-quarter of the physical solution domain was modelled, advantage being taken of the planes of symmetry. Table 1 lists the normalised stress intensity factors, $K_I/\bar{K}$, where $\bar{K} = \sigma\sqrt{\pi b}$ for the range of crack sizes and inclusion geometries considered. For elliptic semi-axes ratio c/a greater than unity, the K_I solutions are only presented for up to certain relative crack sizes as it was found that beyond those sizes, the presence of the inclusion has, to all intents and purposes, no effect on the stress intensity factor. The typical variations of the stress intensity factor with crack size for a given inclusion shape is also shown plotted in Fig. 7.

It can be seen from the results that the shape of the inclusion as well as the mismatch of its shear modulus with that of the matrix material has a very pronounced effect on the stress intensity factor for the crack. Of interest to note is that for a given relative crack size b/c, the stress intensity factor increases as the semi-axes ratio of the elliptical inclusion decreases. Also, given the geometry of the inclusion and the size of the crack, the value of K_I increases as the ratio of the inclusion to matrix shear moduli increases, the rate of increase of K_I with μ_2/μ_1 being greater the smaller the value of c/a.

Problem (II)

In this problem, the elliptical inclusion is partially cracked along one of its axes and the crack also extends into the matrix along the plane of this axis, see Fig. 4. The part-length of the crack in the inclusion is b while that in the matrix is d. In this study, the length d was taken to be equal to c while the length b was varied from $b/2c = 0{\cdot}2$ to $0{\cdot}8$. The body, as before, is subjected to uniaxial tension σ at the remote ends in the direction perpendicular to the plane of the crack. A typical BEM mesh used for solving this problem is shown in Fig. 8;

Table 3b. Normalised modulus of the complex stress intensity factor, $K_o^* = K_o/\bar{K}$, and the phase angle Ψ^* (degrees) for point B in problem (III), $\bar{K} = \sigma\sqrt{\pi d}$; $\Psi^* = \text{Arg}\ (Kd^{-i\epsilon})$

c/a	0	μ_2/μ_1							
		5		10		20		100	
		K_0^*	Ψ^*	K_0^*	Ψ^*	k_0^*	Ψ^*	K_0^*	Ψ^*
	30°	0·842	−20·2	0·855	−20·9	0·860	−21·3	0·845	−21·5
	60°	1·528	−5·2	1·568	−6·0	1·574	−6·4	1·551	−6·5
1/3	90°	1·627	58·2	1·825	60·6	1·983	63·7	2·165	68·3
	120°	0·398	−53·2	0·470	−54·2	0·517	−55·4	0·553	−57·3
	30°	0·881	−19·2	0·907	−20·3	0·917	−21·0	0·913	−21·6
	60°	1·486	−1·1	1·526	−2·3	1·537	−2·9	1·538	−3·4
1/2	90°	1·427	48·5	1·570	49·5	1·658	50·5	1·741	51·5
	120°	0·608	−80·6	0·701	−81·2	0·759	−81·7	0·807	−82·0
	30°	0·963	−10·8	1·005	−12·6	1·028	−13·6	1·058	−14·5
	60°	1·214	13·1	1·281	11·8	1·320	11·0	1·382	10·4
1	90°	1·195	33·1	1·280	32·0	1·329	31·4	1·377	31·1
	120°	1·014	50·5	1·104	49·3	1·157	48·7	1·218	48·1
	30°	0·947	7·0	1·003	5·3	1·035	4·3	1·063	3·5
	60°	1·026	16·2	1·086	14·3	1·120	13·3	1·134	12·4
2	90°	1·059	20·1	1·125	18·2	1·163	17·1	1·196	16·3
	120°	1·083	23·3	1·152	21·3	1·191	20·1	1·223	19·2
	30°	0·920	10·7	0·975	8·8	1·006	7·7	1·019	6·9
	60°	0·986	13·6	1·043	11·5	1·073	10·3	1·066	9·3
3	90°	1·009	15·1	1·069	12·8	1·104	11·4	1·135	10·6
	120°	1·053	16·2	1·116	13·9	1·152	12·5	1·176	11·4

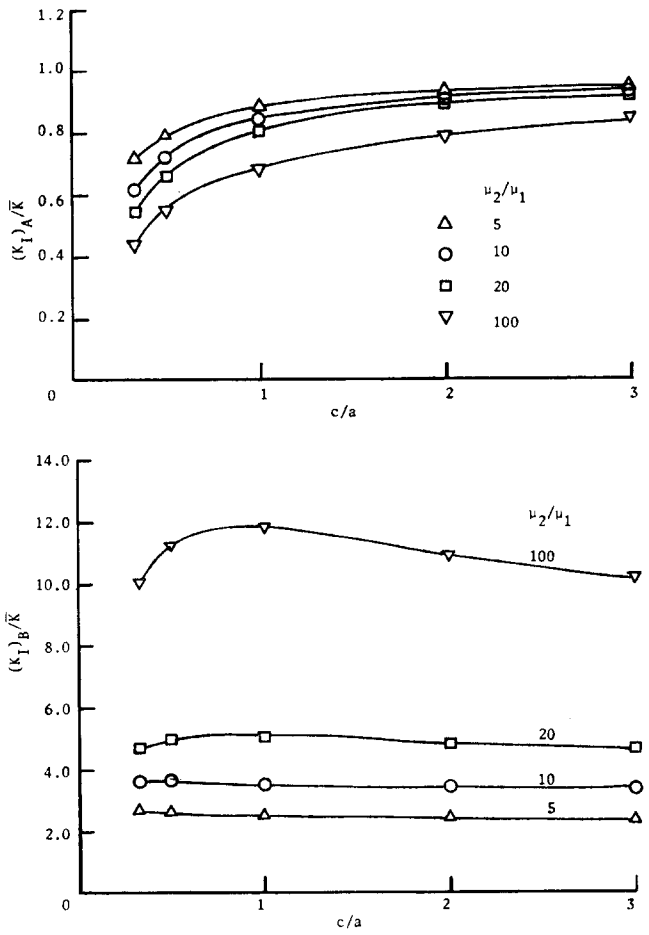

Fig. 9. (a) Variation of $(K_I)_A/\bar{K}$ with c/a; $\bar{K} = \sigma\sqrt{[\pi(b+d)]}$; $b/2c = 0{\cdot}8$. (b) Variation of $(K_I)_B/\bar{K}$ with c/a; $\bar{K} = \sigma\sqrt{[\pi(b+d)]}$; $b/2c = 0{\cdot}8$.

only one-half of the physical problem needs to be modelled as there is a plane of symmetry.

The numerical results from the BEM analysis for the stress intensity factors at the two crack tips, A and B in Fig. 4, are listed in Table 2. The values are normalised with respect to $\bar{K}$, where $\bar{K} = \sqrt{\pi(b+d)}$, and are denoted by $(K_I)_A$ and $(K_I)_B$ for the two points, respectively. Examining first the effects of the inclusion geometry and its material property on the stress intensity factor at the crack-tip A in the matrix, it can be seen that $(K_I)_A/\bar{K}$ decreases as the ratio μ_2/μ_1 increases. Also as c/a increases from 1/3 to 3, $(K_I)_A/\bar{K}$ increases for a given relative crack length $b/2c$.

These trends are exactly opposite from what was observed earlier in Problem (**I**) where the crack-tips are also in the matrix. Figures 9(a) and (b) show, as examples, the variations of these stress intensity factors with the inclusion geometry ratio c/a for a given relative crack size $b/2c$, in this case $b/2c = 0{\cdot}8$. It is worth noting too that the stress intensity factor at A, for all the cases treated here, is always less than that for a crack in an infinite homogeneous body. In contrast, for point B in the inclusion, the values of $(K_I)_B/\bar{K}$ are all significantly greater than unity, suggesting that crack extension in such cracked configurations will occur there first. Also, the variations of $(K_I)_B/\bar{K}$ with the ratios μ_2/μ_1 and c/a are opposite in trends from those for point A.

A special case of this problem, namely, that when the inclusion is circular, has been considered analytically by Erdogan & Gupta.[4] In their treatment, the total length of the crack was kept constant while the proportion of it in the inclusion was varied. Numerical results were presented by them for only one μ_2/μ_1 ratio, namely, 23·077, which corresponds to that for an aluminium inclusion in an epoxy matrix. Although no direct comparison between their results and those presented here can be made, a close comparison is possible for the case $c/a = 1$, $b/2c = 0{\cdot}50$ and $\mu_2/\mu_1 = 20$ considered in this study. Values of $(K_I)_A/\bar{K}$ and $(K_I)_B/\bar{K}$ interpolated from those presented in Ref. 4, are found to be equal to 0·691 and 3·905, respectively, while those obtained from the present BEM analysis are 0·695 and 3·677, as shown in Table 2. Agreement between the BEM and the analytical results is thus very good indeed, the small deviations being attributable to the slightly higher μ_2/μ_1 ratio considered in the analytical study and they are in the right directions as observed earlier on the effects of μ_2/μ_1 changes. The feature of $(K_I)_B$ being significantly greater than $(K_I)_A$ for a given cracked geometry was also seen in the study by Erdogan & Gupta.[4]

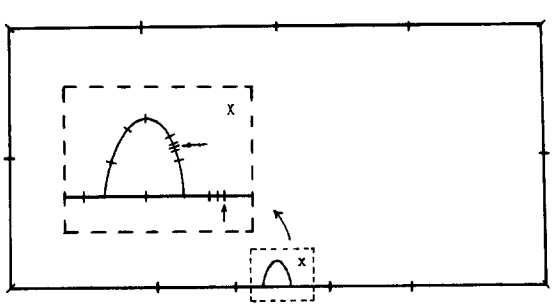

Fig. 10. Typical BEM mesh for Problem (**III**).

Problem (III)

Finally, the last problem considered in this study involves a debonded crack at the interface between the elliptical inclusion and the matrix which is subjected to remote biaxial tension σ. It spans an angle 2θ as shown in Fig. 5 and is symmetric about one of the elliptical axes, continuing into the matrix along the plane of this axis. For the analysis, the length of the straight part of the crack in the matrix, d, was taken to be equal to the length of the semi-axis c and stress intensity factors were calculated for four different values of θ, namely 30°, 60°, 90° and 120°. A typical BEM mesh used here is shown in Fig. 10; it represents one-half of the physical problem. For the crack-tips B at the interface between the two different materials (see Fig. 5), the values K_o and the

phase angle Ψ^* are obtained for the various geometric and material property parameters considered. Tables 3a and 3b present the normalised results of $K_I/\bar{K}$ for the point A and $K_o/\bar{K}$ for the point B from the BEM analysis, respectively; here $\bar{K} = \sigma\sqrt{\pi d}$. Also listed in Table 3a are the corresponding computed values of the non-dimensionalised phase angle Ψ^*, where $\Psi^* = \text{Argument}(Kd^{-i\epsilon})$.

It can be seen from the results that given the cracked configuration, increasing the value of μ_2/μ_1 appears to have the effect of decreasing the stress intensity at point A while generally increasing that at the interface crack-tip B. However this decrease of K_I at crack-tip A becomes relatively small when $c/a > 1$. It is also evident from the numerical results in Table 3b that at the crack-tip B, the values of $K_o/\bar{K}$ and Ψ^* are relatively more sensitive to the inclusion geometry and the extent of the debond at its interface with the matrix than to the mismatch between their material properties. Of perhaps interest to note too is that there are certain sizes of the interface crack, given the geometry of the inclusion, where $\Psi^* = 0$. The value of θ, which is the measure of the size of the interface debond here, at which this occurs is smaller the larger the value of c/a. Although $\Psi^* = 0$ implies that $K_{II} = 0$ in such situations, it should be remarked again that this does not mean that only the opening mode is present in the vicinity of the crack-tip. As has been mentioned earlier, when the material properties are different from one another at the interface crack-tip, the tensile and shear effects are coupled, and K_I and K_{II} do not represent the opening and shear modes as for homogeneous materials.

REFERENCES

1. Cook, T.S. & Erdogan, F. Stresses in bonded materials with a crack perpendicular to the interface, *Int. J. Engng. Sc.*, 1972, **10,** 677–697.
2. Atkinson, C. On the stress intensity factors associated with cracks interacting with an interface between two elastic media, *Int. J. Engng. Sc.*, 1975, **13,** 489–504.
3. Goree, J.G. & Venezia, W.A. Bonded elastic half-planes with an interface crack and a perpendicular intersecting crack that extends into the adjacent material — **I**, *Int. J. Engng. Sc.*, 1977, **15,** 1–17.
4. Erdogan, F. & Gupta, G.D. The inclusion problem with a crack crossing the boundary, *Int. J. Fracture*, 1975, **11,** 13–27.
5. Viola, E. & Piva, A. Fracture behaviour by two cracks around an elliptic rigid inclusion, *Engng. Fracture Mech.*, 1981, **15,** 303–325.
6. Sih, G.C. & Chen, E.P. *Cracks in Composite Materials*, Martinus Nijhoff Pub., 1981.
7. Mura, T. *Micromechanics of Defects in Solids*, Martinus Nijhoff Pub., 1982.
8. Johnson, W.S., ed. Delamination and debonding of materials, *ASTM STP* **876,** 1985.
9. Lee, J.C., Farris, T.N. & Keer, L.M. Stress intensity factors for cracks of arbitrary shape near an interfacial boundary, *Engng. Fracture Mech.*, 1987, **27,** 27–41.
10. Liu, X.H. & Erdogan, F. The crack inclusion interaction problem, *Engng. Fract. Mech.*, 1986, **23,** 821–832.
11. Steif, P.S. A semi-infinite crack partially penetrating a circular inclusion, *J. Appl. Mech.*, Trans. ASME, 1987, **54,** 87–92.
12. Hasebe, N., Okumura M. & Nakamura, T. Stress analysis of a debonding and a crack around a circular rigid inclusion, *Int. J. Fracture*, 1987, **32,** 169–183.
13. Hutchinson, J.W., Mear, M.E. & Rice, J.R. Crack paralleling an interface between dissimilar materials, *J. Appl. Mech.*, Trans. ASME, 1987, **54,** 828–832.
14. Mura, T. Inclusion problems, *Appl. Mech. Reviews*, 1988, **41,** 15–20.
15. England, A.H. An arc crack around a circular inclusion, *J. Appl. Mech.*, Trans. ASME, 1966, **33,** 637–640.
16. Perlman, A.B. & Sih, G.C. Elastostatic problems curvilinear cracks in bonded dissimilar materials, *Int. J. Engng. Sc.*, 1967, **5,** 845–867.
17. Toya, M. A crack along the interface of a circular inclusion embedded in an infinite solid, *J. Mech. Phys. Solids*, 1974, **22,** 325–348.
18. Toya, M. Debonding along the interface of an elliptic rigid inclusion, *Int. J. Fracture*, 1975, **11,** 989–1002.
19. Sendeckyj, G.P. A class of interface crack problems, *ASTM STP*, 1974, **560,** 92–104.
20. Erdogan, F., Gupta, G.D. & Ratwani, M. Interaction between a circular inclusion and an arbitrary orientated crack, *J. Appl. Mech., Trans. ASME*, 1974, **41,** 1007–1013.
21. Selvadurai, A.P.S. & Singh, B.M. On the expansion of a penny-shaped crack by a rigid circular disc inclusion, *Int. J. Fracture*, 1984, **25,** 69–77.
22. Lin, K.Y. & Mar, J.W. Finite element analysis of stress intensity factors for cracks at a bimaterial interface, *Int. J. Fracture*, 1976, **12,** 521–531.
23. Smelser, R.E. Evaluation of stress intensity factors for bimaterial bodies using numerical crack flank displacement data, *Int. J. Fracture*, 1979, **15,** 135–143.
24. Nishioka, T. & Atluri, S.N. Analyses of cracks in adhesively bonded metallic laminates by a 3-D assumed stress hybrid FEM, in *Proc. 22nd AIAA/ASME/ASCE/AHS Structures, Structural Dynamics & Materials Conf.*, Atlanta, April 1981, 66–70.
25. Kuo, A.Y. & Wang, S.S. A dynamic finite element analysis of interfacial cracks in composite, *ASTM STP*, 1985, **876,** 5–34.
26. Sun, C.T. & Jih, C.J. On strain energy release rates for interfacial cracks in bimaterial media, *Engng. Fracture Mech.*, 1987, **28,** 13–20.
27. Sun, C.T. & Manoharan, M.G. Strain energy release rates of an interfacial crack between two orthotropic solids, *J. Composite Materials*, 1989, **23,** 460–478.
28. Matos, P.P.L., McMeeking, R.M., Charalambides & Drory, M.D. A method of calculating stress intensities in bimaterial fracture, *Int. J. Fracture*, 1989, **40,** 235–254.
29. Bhattacharyya, P.K. & Willment, T. Boundary element methods for two-dimensional bimaterial fracture problems, in *Advanced Boundary Element Methods*, ed. T.A. Cruse, Springer-Verlag, 1988, 29–40.
30. Yuuki, R., Cho, S.B., Matsumoto, T. & Kisu, H. Usefulness of Hetenyi's solution for boundary element analysis of crack problems in dissimilar materials, in *Role of Fracture Mechanics in Modern Technology*, eds. G.C. Sih, H. Nisitani and T. Ishihara, Elsevier Science Pub., 1987, 823–834.
31. Yuuki, R. & Cho, S.B. Boundary element analysis of the stress intensity factors for an interface crack in dissimilar materials, in *Boundary Element Methods in Applied*

Mechanics, eds. M. Tanaka and T.A. Cruse, Pergamon Press, 1988, 179–190.
32. Hasegawa, H. A fundamental solution and boundary element method for torsion problems of a bonded dissimilar elastic solid, *ibid*, 139–147.
33. Yuuki, R. & Cho, S.B. Efficient boundary element analysis of stress intensity factors for interface cracks in dissimilar materials, *Engng. Fracture Mech.*, 1989, **34,** 179–188.
34. Lee, K.Y. & Choi, H.J. Boundary element analysis of stress intensity factors for bimaterial interface cracks, *Engng. Fracture Mech.*, 1988, **29,** 461–472.
35. Tan, C.L. & Gao, Y.L. Treatment of bimaterial interface crack problems using the boundary element method, *Engng. Fracture Mech.*, 1990, **36,** 919–932.
36. Cruse, T.A. & Wilson, R.B. Boundary integral equation method for elastic fracture mechanics analysis, AFSOR-TR-78-0355 Report, 1977.
37. Blandford, G.E., Ingrafea, A.R. & Liggert, J.A. Two-dimensional stress intensity factor computations using the boundary element method, *Int. J. Num. Methods Engng.*, 1981, **17,** 387–404.
38. Martinez, J. & Dominguez, J. On the use of quarter-point boundary elements for stress intensity factor computations, *Int. J. Num. Methods Engng.*, 1984, **20,** 1941–1950.
39. Rizzo, F.J. An integral approach to boundary value problems of classical elastostatics, *Q. Appl. Math.*, 1967, **25,** 83–95.
40. Milliams, M.L. The stresses around a fault or crack in dissimilar media, *Bull. Seismological Soc. America*, 1959, **49,** 199–204.
41. Comninou, M. The interface crack, *J. Appl. Mech., Trans.*, 1977, **44,** 631–636.
42. Rice, J.R. Elastic fracture mechanics concepts for interfacial cracks, *J. Appl. Mech., Trans. ASME*, 1988, **55,** 98–103.
43. Rice, J.R. & Sih, G.C. Plane problems of cracks in dissimilar media, *J. Appl. Mech., Trans. ASME*, 1965, **32,** 418–423.
44. Hong, C.C. & Stern, M. The computation of stress intensity factors in dissimilar materials, *J. Elasticity*, 1978, **8,** 21–34.